Influence of off-Sun-Earth line distance on the accuracy of L1 solar wind monitoring

S. E. Milan[1,2]*, J. A. Carter[1], G. E. Bower[1], A. L. Fleetham[1], and B. J. Anderson[3]

[1]Department of Physics and Astronomy, University of Leicester, Leicester, UK.
[2]Birkeland Centre for Space Sciences, University of Bergen, Norway.
[3]Johns Hopkins University Applied Physics Laboratory, Laurel, Maryland, USA.

Key Points:

- We compare OMNI measurements of IMF B_Y by Wind with associated variations in the dayside ionosphere
- The cross-correlation between these measurements deteriorates as the off-Sun-Earth line distance of Wind increases
- A delay of around 17 minutes is found between OMNI predictions of arrival at the bow shock and the ionospheric response

*Department of Physics and Astronomy, University of Leicester, Leicester LE1 7RH, UK

Corresponding author: Steve Milan, steve.milan@le.ac.uk

Abstract

Upstream solar wind measurements from near the L1 Lagrangian point are commonly used to investigate solar wind-magnetosphere coupling. The off-Sun-Earth line distance of such solar wind monitors can be large, up to 100 R_E. We investigate how the correlation between measurements of the interplanetary magnetic field and associated ionospheric responses deteriorates as the off-Sun-Earth line distance increases. Specifically, we use the magnitude and polarity of the dayside region 0 field-aligned currents (R0 FACs) as a measure of IMF B_Y-associated magnetic tension effects on newly-reconnected field lines, related to the Svalgaard-Mansurov effect. The R0 FACs are derived from Advanced Magnetosphere and Planetary Electrodynamics Response Experiment (AMPERE) measurements by a principal component analysis, for the years 2010 to 2016. We perform cross-correlation analyses between time-series of IMF B_Y, measured by the Wind spacecraft and propagated to the nose of the bow shock by the OMNI technique, and these R0 FAC measurements. Typically, in the summer hemisphere, cross-correlation coefficients between 0.6 and 0.9 are found. However, there is a reduction of order 0.1 to 0.15 in correlation coefficient between periods when Wind is close to (within 45 R_E) and distant from (beyond 70 R_E) the Sun-Earth line. We find a time-lag of around 17 minutes between predictions of the arrival of IMF features at the bow shock and their effect in the ionosphere, irrespective of the location of Wind.

Plain Language Summary

Space weather within the Earth's geospace environment is driven by the interaction of the solar wind with the magnetosphere. Measurements of the solar wind upstream of the Earth are crucial for understanding this interaction and for providing some advanced warning of hazardous conditions about to arrive. Such measurements are typically made by spacecraft located in orbit about the L1 Lagrangian point, sometimes far from the Sun-Earth line, and it is uncertain how representative these measurements are of the solar wind that actually hits the Earth. In this study we investigate how predictions degrade as the off-Sun-Earth line distance increases. We use measurements of the east-west component of the interplanetary magnetic field measured by the Wind spacecraft and observations of magnetic field-aligned electrical currents within the magnetosphere, to assess how well these are correlated. We find that the correlation does indeed decrease somewhat as Wind wanders far from the Sun-Earth line. This study will help provide confidence in using these upstream monitors, but also allow quantification of what discrepancies can be expected. It also allows the scale-size of features in the solar wind to be estimated.

1 Introduction

Upstream solar wind monitoring is invaluable for studies of the relationship between conditions within the interplanetary medium and dynamics within the Earth's magnetosphere, and for forecasting upcoming geomagnetic activity. Ideally, spacecraft just ahead of the bowshock, or even within the magnetosheath, can give measurements of the plasma characteristics and magnetic field that are about to impinge on the magnetopause. However, orbital dynamics prevent spacecraft station-keeping in such ideal locations, and spacecraft so close to the magnetopause do not provide much advanced warning of incoming space weather hazards. A compromise is to place spacecraft in orbit about the L1 Lagrangian point, such that they can be kept in front of the magnetosphere, providing measurements of the solar wind which will impact the magnetosphere in approximately one hour's time. Such spacecraft have included Wind, the Advanced Composition Explorer (ACE), and the Deep Space Climate Observatory (DSCOVR). Goddard Space Flight Centre developed the OMNI dataset, which assesses the speed and orientation of features within the solar wind measured by these and other spacecraft, and time-lags the obser-

vations to the point of impact on the bow shock (King & Papitashvili, 2005). This dataset has been instrumental in advancing our understanding of the interaction of the solar wind with the magnetosphere. However, the spacecraft providing these observations can wander up to 100 R_E from the Sun-Earth line, such that it is unclear how representative their measurements are of the solar wind which will actually arrive at the magnetosphere (e.g., Crooker et al., 1982; Collier et al., 1998; Case & Wild, 2012). It is the purpose of this paper to investigate how the predictive capability of solar wind monitoring deteriorates as the off-Sun-Earth line distance increases.

To assess the accuracy of the upstream measurements, some ground-truth is necessary: an observable that is thought to accurately reflect conditions within the solar wind that is interacting with the magnetopause. In this study we use the Svalgaard-Mansurov effect, in which field-aligned and ionospheric currents within the cusp region react to the B_Y component of the interplanetary magnetic field (IMF), and produce DPY magnetic perturbations on the ground (Svalgaard, 1973; Mansurov, 1969; Friis-Christensen et al., 1972; Jørgensen et al., 1972; Cowley et al., 1991). Milan et al. (2015, 2017) showed that principal component analysis (PCA) could be used to automatically extract the polarity and magnitude of the field-aligned currents (FACs) associated with this effect from observations of the global FAC pattern by the Advanced Magnetosphere and Planetary Electrodynamics Response Experiment or AMPERE (Anderson et al., 2000, 2002; Waters et al., 2001, 2020). We refer to this as the region 0 (R0) FAC to distinguish it from the region 1 and region 2 (R1/R2) FACs first identified by Iijima and Potemra (1976). Milan et al. (2018) refined the procedure by applying PCA separately to just the dayside portion of the FAC patterns. They demonstrated that the polarity of the currents switched promptly when there were sharp reversals in IMF B_Y at the nose of the bow shock as predicted by OMNI, with a time-lag of between 10 and 20 minutes. This time-lag is interpreted as the propagation delay associated with traversal of the magnetosheath by the shocked solar wind and one or two Alfvén travel-times from the magnetopause to the ionosphere. Moreover, the association between R0 FAC polarity and IMF B_Y held irrespective of whether IMF B_Z was directed southwards or northwards. Hence, we consider the magnitude and polarity of the R0 FAC, extracted using the PCA technique of Milan et al. (2018), to be a good indicator of the sense of IMF B_Y at the magnetopause.

We perform a cross-correlation analysis between IMF B_Y observed by the Wind spacecraft and the R0 FAC extracted from AMPERE data for the period 2010 to 2016. The Wind spacecraft orbited the L1 point in an elliptical orbit varying periodically in off-Sun-Earth line distance, $R_{YZ} = (Y^2 + Z^2)^{1/2}$, between 30 R_E and 100 R_E, where Y and Z are GSE coordinates. We determine how the cross-correlation deteriorates as R_{YZ} increases.

2 Methodology and observations

AMPERE inverts magnetic perturbations observed by the 66 spacecraft of the Iridium constellation to determine the global distribution of field-aligned currents (FACs) across the northern and southern hemispheres on a geomagnetic grid with 24 magnetic local time (MLT) sectors and 50 one-degree magnetic colatitude bins, with a cadence of 2 minutes (Anderson et al., 2000, 2002; Waters et al., 2001; Coxon et al., 2018). The morphology of the FACs responds to changes in upstream solar wind and IMF conditions, to changes in magnetotail processes, and to changes in the magnetic open flux content of the magnetosphere (Clausen et al., 2012; Milan et al., 2018). Analysing this feature-rich dataset can be difficult. As an exercise in dimensionality-reduction, Milan et al. (2015) applied principal component analysis (PCA) to the FAC patterns to find the set of basis-vectors ("eigenFACs") that best represent the variability within the data. It was found that the most significant eigenFAC represented the R1/R2 current system (Iijima & Potemra, 1976) and the second-most the R0 system. The analysis was improved by Milan et al. (2018) in that FACs sunwards and antisunwards of the dawn-dusk meridian were anal-

ysed separately, and two sets of eigenFACs computed, recognising that dayside and nightside processes are largely decoupled. It is this second method that we employ in this study, concentrating solely on the dayside FACs.

The PCA technique is described in detail by Milan et al. (2015, 2018), but we reprise it here briefly for completeness. Each 2-min AMPERE map comprises 1200 FAC density values on a 25×50 grid. First, each map is normalised to remove the influence of changing polar cap size (Clausen et al., 2012): the centre of the FAC pattern is found, a circle is fitted to the boundary between the R1 and R2 FACs, and then each map is rescaled to a common size. Each pre-processed map (of which there are nearly two million for each hemisphere) is represented as a vector of data values and all the individual vectors are stacked together to form a matrix. This matrix is multiplied by its transpose to find the covariance matrix of the dataset. The eigenvectors of this covariance matrix are the dominant patterns of variability within the data (the eigenFACs) and their corresponding eigenvalues indicate their significance in explaining this variability. To find the contribution of a particular eigenFAC to an individual map, the inner product or "overlap" between the two is computed: in the case of the second eigenFAC, which corresponds to the R0 FAC system, this overlap is referred to as α_2 (which has arbitrary units). This then formed our primary magnetospheric observable. Measurements from both the northern and southern hemispheres (NH and SH) were available.

The OMNI dataset employs observations from a range of upstream solar wind monitors to predict the solar wind and IMF conditions at the nose of the bow shock by computing an expected propagation delay from the spacecraft location and time-lagging the data. A long time-series of standard OMNI data may come from several different spacecraft located at different distances from the magnetosphere. However, the OMNI dataportal also provides access to data from an individual spacecraft (`https://omniweb.gsfc.nasa.gov/ow_min.html`): to simplify analysis, in this study we use data from Wind alone. The primary parameter we used is the GSM B_Y component of the IMF. This is provided at 1-min cadence, but we down-sampled this to 2-min to match the AMPERE observations.

Figure 1 shows the dependence of NH α_2 on IMF B_Y for the period 2010 to 2016, subdivided by month. A clear positive linear correlation between the two is found, indicating that the polarity and magnitude of the R0 FACs is controlled by B_Y-related tension forces on newly-reconnected field lines. This is clearly true for both northwards and southwards IMF conditions. The slope of the fit is greatest in summer months and becomes almost zero in January and December. This seasonal dependence is thought to be mainly controlled by the ionospheric conductance at the footprint of the R0 FACs, produced by solar illumination. As the conductance increases in summer there is greater frictional coupling between the ionosphere and neutral atmosphere, and hence more intense FACs are required to transmit stress from the magnetopause to the ionosphere. However, as noted by Milan et al. (2001), East-West variations in the dayside ionospheric convection throat are less pronounced in winter than in summer, so the R0 seasonal variation may also reflect hemispheric differences in dayside solar wind-magnetosphere-ionosphere coupling. We use α_2, especially in summer months as an indicator of IMF B_Y at the magnetopause. Similar results are found for the SH (not shown), except that the slope is negative as the polarity of the SH R0 FACs is opposite to the sense of B_Y. In this case, the slope of the relationship maximises in SH summer, i.e., December and January, though the slope is weaker in the SH than in the NH. It is known that the SH FACs are in general weaker than in the NH (Coxon et al., 2016; Milan et al., 2017), and this is borne out in these results.

Any small gaps in the α_2 and B_Y time-series were linearly interpolated over. We divided the α_2 and B_Y time-series into separate windows, each N data-points in length, and calculated the cross-correlation between the two, noting the peak correlation coefficient value and the lag at which this peak occurred. The analysis was then repeated,

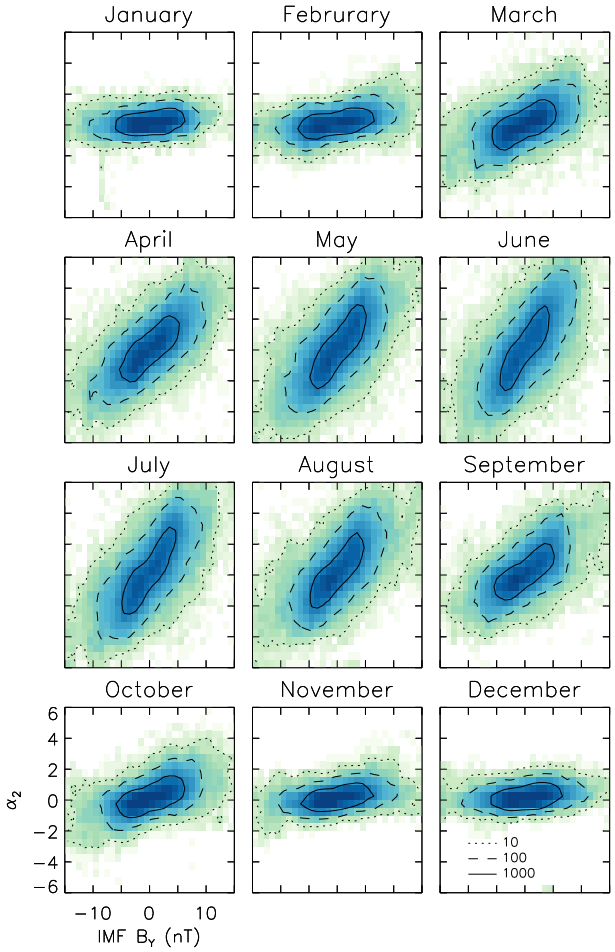

Figure 1. The occurrence distributions showing the relationship between the northern hemisphere α_2 coefficient and IMF B_Y in bins 1 nT wide and 0.5 (arbitrary units) high, for the months January to December, 2010 to 2016. The occurrence is shown on a logarithmic scale, contours indicating 10, 100, and 1000 occurrences per bin.

with the window stepped on by $N/2$ data-points each time, for the 7-year period (2010 to 2016) for which AMPERE data is currently available. We selected the optimum value of N by trying a range of different values. Values of N between approximately 500 and 900 maximised the cross-correlation, with a broad peak. We selected $N = 720$ (1 day) because this meant that dipole angle (controlling solar insolation of the cusp region ionosphere) averaged out over the window. Smaller values of N would have lead to diurnal variations in the cross-correlation coefficient. With $N = 720$, there were 5114 possible cross-correlation windows; once data gaps from Wind or AMPERE were factored in, 4587 remained. We note that the exact choice of N does not alter the subsequent findings of this study.

The results of the analysis for the NH are presented in Figure 2. The top panel shows the maximum correlation coefficient from the cross-correlation analysis in grey; a 10-day (20-point) running mean is shown in black. The middle panel shows the lag with the maximum correlation, with the marginal distribution shown to the right. The bottom panel shows the location of the Wind spacecraft in GSE coordinates. The spacecraft was in an elliptical orbit about L1, varying in X between approximately 200 and 260 R_E, in Z between ± 20 R_E, and in Y between ± 100 R_E. As a consequence, the distance off the Sun-Earth line, $R_{YZ} = (Y^2 + Z^2)^{1/2}$, varied between approximately 25 and 100 R_E, about 4 times a year.

The peak correlation between α_2 and B_Y varied between 0.9 and -0.2 (the running mean between 0.8 and 0.2), maximising in summer months due to the R0 current magnitudes being greatest at these times. The running mean was close to 0.7 in summer. The lag of peak correlation showed a broad peak between 10 and 30 mins, with a maximum near 17 mins; the range increased in winter months when the correlation coefficient was small and clustered near 17 mins in summer months (with a few exceptions, see below). In the top panel, vertical, red dashed lines show the times when R_{YZ} maximised, and there appears to be, on average, a reduction in the running-mean of the correlation coefficient by about 0.1 at these times.

A Fourier analysis of the correlation time-series indicates peaks in the spectrum at 365 days (1 year), 183 days (half a year), 150 days, and 88 days (the frequency of variation of R_{YZ}). A reconstruction of the time-series using the first 3 peaks is shown in green (offset for clarity) and including the 88 day component in blue. Although the effect is small, there is clearly a reduction in the correlation around the maxima in R_{YZ}. The 365 day period reflects the seasonal variation in the correlation and the 183 day period appears as the summer maxima are wider than the winter minima. It is unclear what gives rise to the 150 day period.

Ten representative intervals, along with their peak correlation and peak lag, have been highlighted by red dots. The associated IMF B_Y (red) and α_2 (black) time-series are presented in Figure 3. In the majority of cases there is a close correspondence between B_Y and the polarity and magnitude of the R0 FAC. However, each panel highlights some typical features within the correlations which we now discuss.

(a) The correlation is high, but at times the variation in the R0 FAC appears to precede those in B_Y, and a peak lag of -12 mins is found. (b) Variations in B_Y are rapid and some short-duration features are not well-captured by α_2; this may indicate a smoothing effect in the magnetospheric response to rapid B_Y changes. A time-lag of 18 mins is found. (c) In this example, short-duration negative excursions in B_Y are also present in α_2, with a consistent time-lag near 16 mins. (d) Although there are significant variations in B_Y, α_2 is near-zero throughout; this interval comes from near the winter solstice, when the R0 FAC is almost absent from the dayside currents. (e) There are relatively long duration changes in B_Y; although some of these excursions are present also in α_2, some features are absent, for example around data points 200 and 360, and as a consequence a relatively long time lag of 24 mins is found. (f) Overall, the correlation

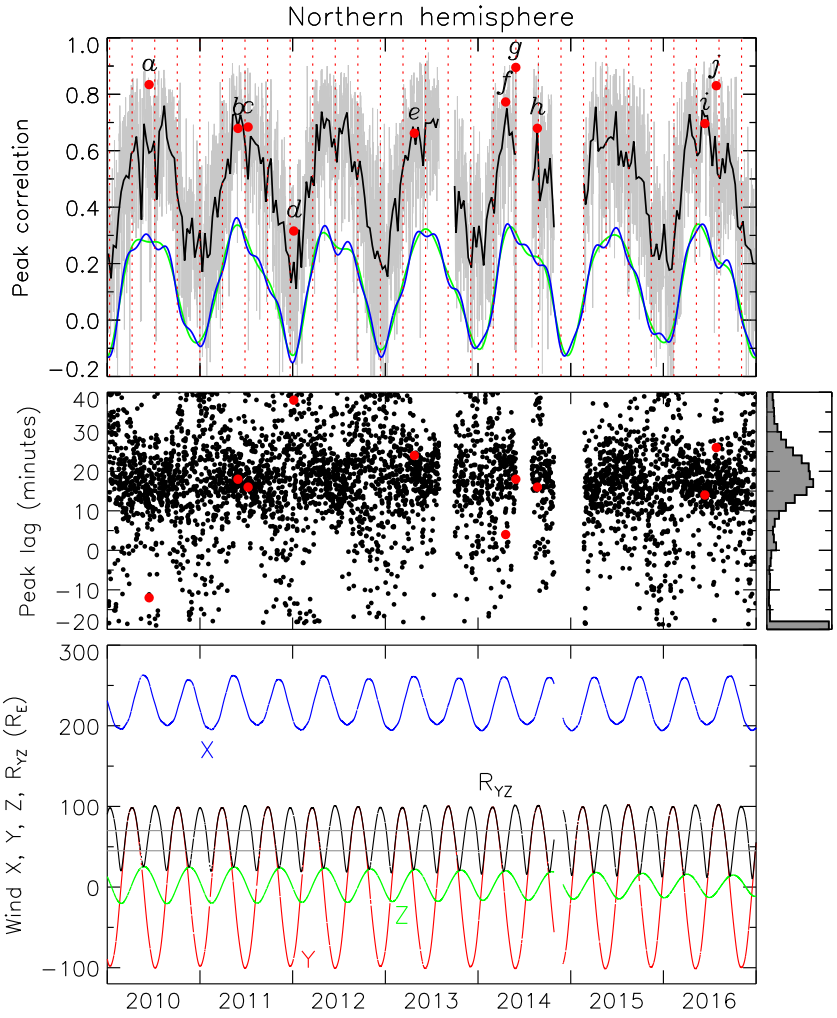

Figure 2. (Top) The peak cross-correlation coefficient between NH α_2 and IMF B_Y every 12 hours (grey), and a 10-day running mean (black). The green and blue curves are reconstructions of the correlation time series using a Fourier expansion in 3 and 4 terms, respectively (see text for details), displaced vertically for clarity. Vertical red, dashed lines indicate times that the Wind spacecraft was furthest from the Sun-Earth line. (Middle) The lag associated with the peak in the cross-correlation. The marginal distribution is shown to the right; the bottom bar indicates the proportion of correlations in which the lag of peak correlation was outside the -20 to 40 min range. (Bottom) The position of the Wind spacecraft in GSE X (blue), Y (red), and Z (green). The distance from the Sun-Earth line, R_{YZ} is shown in black. Red dots in the figure correspond to panels in Figure 3.

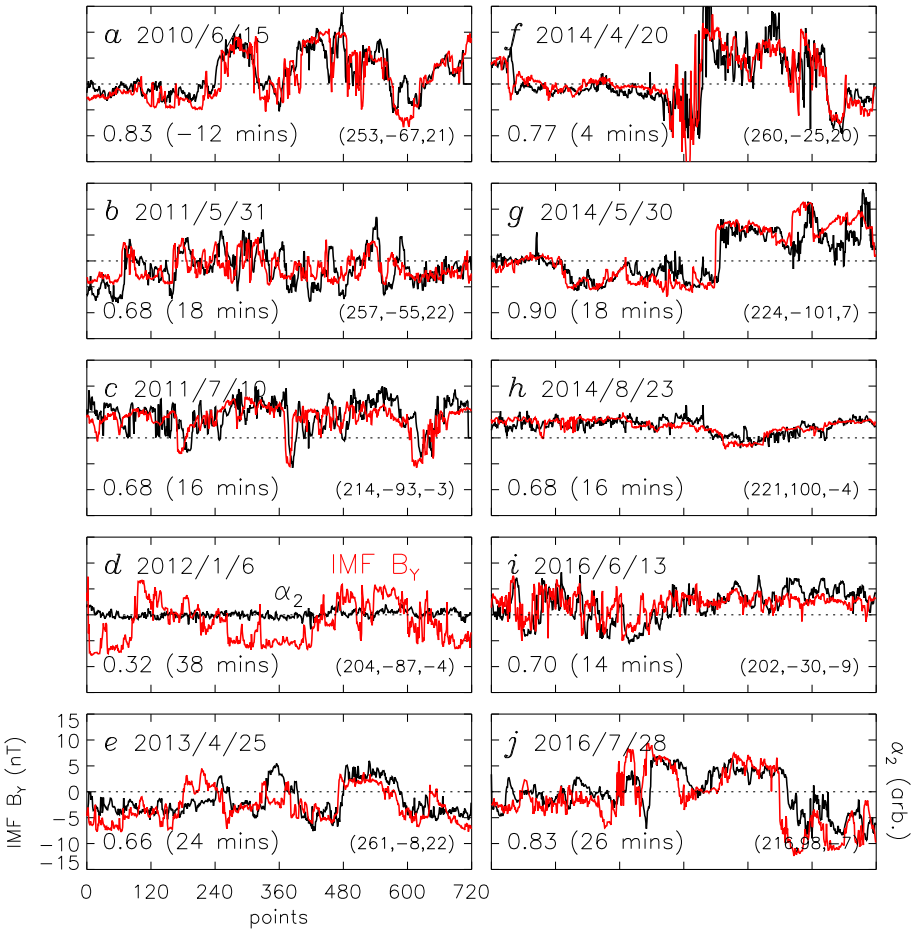

Figure 3. Ten selected correlations, highlighted by red dots in Figure 2. Each panel corresponds to 24 hours of data (720 data points). IMF B_Y (GSM) observed at Wind is shown in red, the α_2 parameter in black; α_2 is shown on an arbitrary scale, though it is the same in each panel. The top-left in each panel indicates the date of the observations, the bottom-left the peak correlation coefficient and peak lag, and the bottom-right the approximate (X, Y, Z) GSE coordinates of Wind.

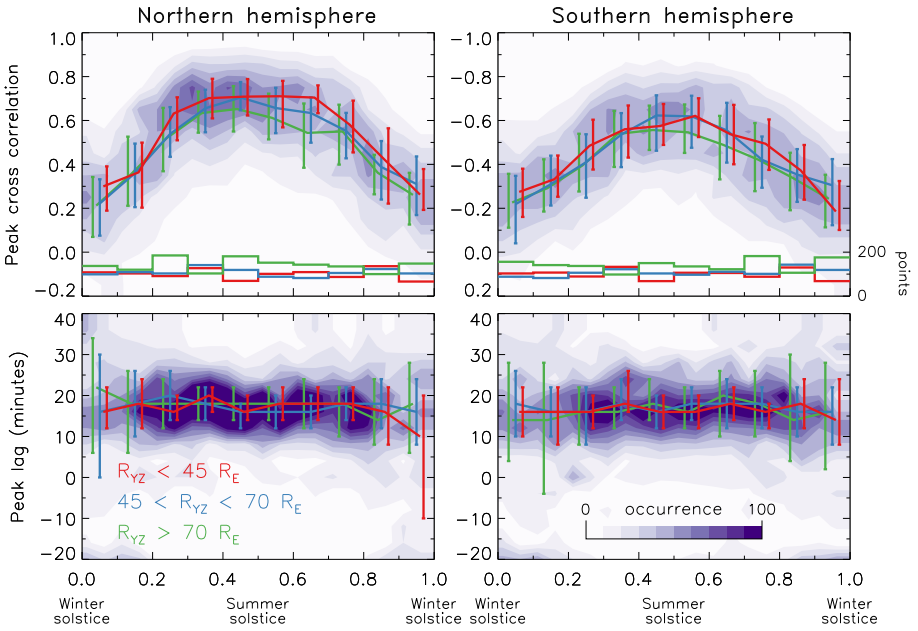

Figure 4. Combined seasonal dependence of peak cross-correlation (top panels) and peak lag (bottom panels) between IMF B_Y and α_2, for the years 2010 to 2016 in the northern hemisphere (left panels) and southern hemisphere (right panels). Shading shows the overall occurrence distribution. The median and quartiles of the distributions for off-Sun-Earth line distances $R_{YZ} < 45R_E$, $45 < R_{YZ} < 70R_E$, and $R_{YZ} < 70R_E$ are shown in red, blue, and green. The number of points in each year-fraction bin is indicated in the lower portion of the top panels.

is high but although there is a clear lag between B_Y and α_2 at the start of the interval, no lag is apparent at the end, and an overall lag of 4 mins is found. (g) The overall correlation is high, but some discrepancy is seen after data point 540. (h) Only slow variations in B_Y are seen at Wind and these are reflected in α_2. (i) Some rapid fluctuations in B_Y are not present in α_2 and towards the end of the interval some fluctuations are seen in α_2 but not B_Y. (j) Long-duration variations in B_Y are also seen in α_2, but the timings are quite variable, and a relatively long lag is calculated.

Figure 4 shows the correlation data, peak correlation in the top panels and peak lag in the bottom panels, for both the northern and southern hemispheres as a function of time of year (year-fraction from winter solstice to winter solstice). The shading shows the occurrence distribution of the full data set. The data are then subdivided by the distance of Wind from the Sun-Earth line, R_{YZ}, in ranges of less than 45 R_E (red), between 45 and 70 R_E (blue), and greater than 75 R_E (green). These ranges were selected such that similar numbers of correlations fell in 10 equal-width year-fraction bins (the occurrences are shown in the lower portions of the top panels); these ranges are shown as horizontal grey lines in the lower panel of Figure 2. The median and upper and lower quartiles of peak correlation and peak lag are then calculated in each bin, and shown as the coloured curves and vertical bars. The peak correlations in the NH and SH are positive and negative, respectively, due to the polarity of the R0 FACs in the two hemispheres.

The correlations are a minimum in winter and a maximum in summer, due to the weakness of the R0 FACs when there is little solar insolation. The median peak correlation in summer is 0.7 in the NH and 0.6 in the SH; the summer NH peak is higher and broader than that in the SH. We attribute the discrepancy between the two hemispheres to two factors: (a) it is known that the FACs measured by AMPERE are overall weaker

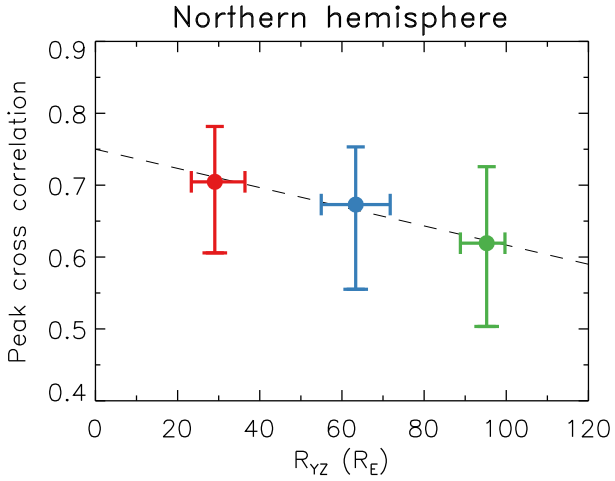

Figure 5. The reduction in median peak correlation with off-Sun-Earth line distance, R_{YZ}. Vertical and horizontal bars show the quartiles within the bins $R_{YZ} < 45R_E$, $45 < R_{YZ} < 70R_E$, and $R_{YZ} < 70R_E$. Only correlations between year-fractions of 0.3 and 0.7 are included in the analysis.

in the SH than the NH (Coxon et al., 2016; Milan et al., 2017), though the reasons for this are still unknown; (b) the orbital configuration of the Iridium spacecraft is sub-optimal in the SH (Waters et al., 2020), such that small-scale FACs (including R0) may be poorly sampled. The peak lag distribution maximises near 17-18 minutes at all times of year, though it broadens around winter solstice when the correlations are poor.

Our main finding is that the peak correlation depends on R_{YZ}, such that as Wind moves further from the Sun-Earth line the correlation decreases, especially in the NH. We focus on year-fractions between 0.3 and 0.7, the broad summer maximum. The difference in the median correlation coefficient between the $R_{YZ} < 45R_E$ and $R_{YZ} > 70R_E$ bins is of order 0.1, as seen in Figure 5. The difference between the upper and lower quartiles also increases marginally with greater R_{YZ}. A linear fit to the data suggests that if measurements were available at $R_{YZ} = 0$, then the decrease in correlation coefficient at $R_{YZ} = 100R_E$ would be of order 0.15. On the other hand, there is little discernible difference in the peak lags in the different R_{YZ} ranges.

Similar analyses were attempted, expect binning the data by Wind X or Y. Unfortunately, the period of the Wind orbit, being close to 6 months, precluded a uniform sampling across the different seasons. What results were obtained suggested that the upstream distance, X, makes little difference to the correlations, and that the Y location, either ahead of Earth in its orbit or behind, did not change the results found in Figure 4.

3 Discussion and Conclusions

There has been debate regarding the validity of L1 observations of the solar wind for understanding solar wind-magnetosphere coupling, especially when monitors are a long distance from the Sun-Earth line. We have used the magnitude and polarity of the R0 field-aligned currents derived from AMPERE observations as ground-truth for the predictions by OMNI (specifically from the Wind spacecraft) of the B_Y component of the IMF that impacts the magnetosphere. The measured parameter we have used is the α_2 component derived from a principal component analysis of the FACs (Milan et al.,

2015, 2017, 2018). This ground-truth is only applicable in summer months as the R0 FACs are weak around winter solstice due to a lack of solar insolation and a possible seasonal dependence in the East-West asymmetry of the dayside convection throat (Milan et al., 2001). We have shown that the cross-correlation between IMF B_Y and α_2 decreases as the off-Sun-Earth line distance, R_{YZ}, increases. The reduction in peak cross-correlation coefficient is around 0.1 to 0.15. We also find a relatively consistent time-lag between variations in IMF B_Y and α_2 of between 15 and 20 minutes on average. This lag is interpreted as the communication-time between solar wind changes at the bow shock (the predicted timing given by the OMNI technique) and the ionosphere, comprising the propagation delay across the magnetosheath and some Alfvén travel-time from the magnetopause and the ionosphere. Significantly longer or shorter time lags, or even negative time lags (Figure 3a), indicate that an incorrect propagation delay was calculated by the OMNI technique. Such discrepancies could be produced by the assumption that solar wind features have planar boundaries, especially if R_{YZ} is large. However, we do not see a significant change in timing with R_{YZ}.

Khan and Cowley (1999) estimated that the delay between solar wind features arriving at the bow shock nose and the associated response in the ionosphere should be of order 5 to 15 mins, possibly with some systematic offset. Our finding of a delay of 15 to 20 mins could indicate that this systematic offset is approximately 10 mins. It may also reflect the time that the R0 FACs take to respond to changes in IMF B_Y, occupying as they do an area in the ionosphere of up to 10° of latitude by 3-4 hours of MLT (Milan et al., 2015). Alternatively, the systematic delay could be due to the AMPERE technique itself, in which the Iridium spacecraft take approximately 10 mins to traverse their $\sim 30°$ latitudinal separation around each orbital plane.

While many studies have focussed on the timing of solar wind features (Crooker et al., 1982; Collier et al., 1998; Case & Wild, 2012), here we have mainly studied the fidelity between solar wind measurements from far upstream and the response within the magnetosphere; in other words, these correlations have been filtered through the solar wind-magnetosphere coupling process. Despite this, the correlations can be high (of order 0.9) even when rapid and short duration fluctuations appear in IMF B_Y, indicating that the magnetospheric response can be prompt and linear, during both northwards and southwards IMF conditions. In general, the median correlation is about 0.7 in summer months, indicating that the response is not always so exact. The results reported are clearer in the northern hemisphere than in the southern hemisphere, though we anticipate that this is due to stronger FACs being observed in the NH and a less optimal orbital configuration of AMPERE in the SH. This does suggest, however, that the correlation coefficients will be limited by the spatial and temporal resolution of the AMPERE technique and our method of extracting the R0 FACs from a complicated data set.

Putting limitations of the technique to one side, lower correlation coefficients can arise for several reasons, including a lack of fidelity between measurements at L1 and in the ionosphere, i.e. short-duration features that are seen in B_Y but not in α_2 and *vice versa* (e.g., Figure 3e and i), or changes in the lag between the two within a 24 hour window (e.g., Figure 3a and f). However, individual cases of these discrepancies are not necessarily due to large R_{YZ}: high correlations can be found when Wind is far from the Sun-Earth line (Figure 3a and g) and poorer correlations when Wind is near the Sun-Earth line (Figure 3e). Visual inspection of Figure 2 does seem to suggest that there are dips in correlation correlation of about 0.1 to 0.2 when Wind is at it's maximum distance from the Sun-Earth line, though the temporal width of these dips is quite variable. This corroborates the changes in median correlation with increasing R_{YZ} shown in Figures 4 and 5.

Collier et al. (1998) studied the solar wind propagation delay from a spacecraft far upstream of the Earth and one just outside the bow shock. By comparing their timings

with similar ones made by Crooker et al. (1982), they suggested that there might be a solar cycle dependence of the orientation of features in the solar wind and hence the accuracy of predicted propagation delay. However, although our observations span over half a solar cycle (albeit a relatively weak cycle), from examination of Figure 2 we see no evidence for such a dependence in our correlations.

R_{YZ} varies between about 25 and 100 R_E. The reduction in correlation when R_{YZ} is large suggests that there is structure within the solar wind transverse to the flow direction on spatial scales of 100 R_E. Crooker et al. (1982) estimated the coherence scale length of features in the solar wind to be of order 90 R_E, which is approximately consistent with our findings. On the other hand, the structure along the flow direction is known to be as small as 10 R_E, corresponding to temporal variations in the OMNI data of a few minutes.

Many authors have developed coupling functions for the solar wind-magnetosphere interaction (e.g., Newell et al., 2007; Milan et al., 2012; Lockwood & McWilliams, 2021, and references therein). Accurate characterisation of the upstream solar wind conditions is crucial for such studies. The problems with solar wind monitors identified in the present study suggests that there is an intrinsic limit to the predictive capability of such coupling functions.

A similar study could have been undertaken with ground-based magnetometers, looking for magnetic perturbations produced by the horizontal ionospheric closure currents associated with the R0 FACs, or ionospheric radars looking at the east-west sense of the dayside convection throat. Both methods would have suffered from non-continuous data (neither magnetometers nor radars remain located in the cusp sector), and it would have been much less straightforward to remove the effect of latitudinal changes in the position of the cusp. We have also been able to exploit the fact that the polarity of the R0 FACs seems independent of whether the IMF is directed northwards or southwards, whereas the convection geometry changes markedly under these two conditions.

We conclude that solar wind measurements up to 100 R_E off the Sun-Earth line are valuable for studies of solar wind-magnetosphere coupling. Discrepancies between IMF variations and their ground signature, and the timing between these, can be found for all values of R_{YZ}. However, a reduction in the overall fidelity of predictions of IMF features does occur as this distance increases. We have quantified this as a reduction in cross-correlation coefficient between measurements near L1 and in the ionosphere of between 0.1 and 0.15 in time-series of 24 hour duration.

Acknowledgments

SEM and JAC were supported by the Science and Technology Facilities Council (STFC), UK, grant no. ST/S000429/1; GEB and ALF were supported by STFC studentships. The work at the Birkeland Centre for Space Centre, University of Bergen, Norway, was supported by the Research Council of Norway/CoE under contract 223252/F50. We thank the AMPERE team and the AMPERE Science Center for providing the Iridium-derived data products; AMPERE products are available at `http://ampere.jhuapl.edu`. The OMNI data were obtained from the GSFC/SPDF OMNIWeb interface at `http://omniweb.gsfc.nasa.gov`.

References

Anderson, B., Takahashi, K., Kamei, T., Waters, C., & Toth, B. (2002). Birkeland current system key parameters derived from Iridium observations: Method and initial validation results. *Journal of Geophysical Research: Space Physics*, *107*(A6), SMP–11. doi: https://doi.org/10.1029/2001JA000080

Anderson, B., Takahashi, K., & Toth, B. (2000). Sensing global Birkeland currents

with Iridium® engineering magnetometer data. *Geophysical Research Letters*, *27*(24), 4045–4048. doi: https://doi.org/10.1029/2000GL000094

Case, N., & Wild, J. (2012). A statistical comparison of solar wind propagation delays derived from multispacecraft techniques. *Journal of Geophysical Research: Space Physics*, *117*(A2). doi: https://doi.org/10.1029/2011JA016946

Clausen, L., Baker, J., Ruohoniemi, J., Milan, S., & Anderson, B. (2012). Dynamics of the region 1 Birkeland current oval derived from the Active Magnetosphere and Planetary Electrodynamics Response Experiment (AMPERE). *Journal of Geophysical Research: Space Physics*, *117*(A6). doi: https://doi.org/10.1029/2012JA017666

Collier, M. R., Slavin, J., Lepping, R., Szabo, A., & Ogilvie, K. (1998). Timing accuracy for the simple planar propagation of magnetic field structures in the solar wind. *Geophysical Research Letters*, *25*(14), 2509–2512. doi: https://doi.org/10.1029/98GL00735

Cowley, S., Morelli, J., & Lockwood, M. (1991). Dependence of convective flows and particle precipitation in the high-latitude dayside ionosphere on the x and y components of the interplanetary magnetic field. *Journal of Geophysical Research: Space Physics*, *96*(A4), 5557–5564. doi: https://doi.org/10.1029/90JA02063

Coxon, J., Milan, S., & Anderson, B. (2018). A review of Birkeland current research using AMPERE. *Electric Currents in Geospace and Beyond*, 257–278. doi: https://doi.org/10.1002/9781119324522.ch16

Coxon, J., Milan, S., Carter, J., Clausen, L., Anderson, B., & Korth, H. (2016). Seasonal and diurnal variations in AMPERE observations of the Birkeland currents compared to modeled results. *Journal of Geophysical Research: Space Physics*, *121*(5), 4027–4040. doi: https://doi.org/10.1002/2015JA022050

Crooker, N., Siscoe, G., Russell, C., & Smith, E. (1982). Factors controlling degree of correlation between isee 1 and isee 3 interplanetary magnetic field measurements. *Journal of Geophysical Research: Space Physics*, *87*(A4), 2224–2230. doi: https://doi.org/10.1029/JA087iA04p02224

Friis-Christensen, E., Lassen, K., Wilhjelm, J., Wilcox, J., Gonzalez, W., & Colburn, D. (1972). Critical component of the interplanetary magnetic field responsible for large geomagnetic effects in the polar cap. *Journal of Geophysical Research*, *77*(19), 3371–3376. doi: https://doi.org/10.1029/JA077i019p03371

Iijima, T., & Potemra, T. (1976). The amplitude distribution of field-aligned currents at northern high latitudes observed by Triad. *Journal of Geophysical Research*, *81*(13), 2165–2174. doi: https://doi.org/10.1029/JA081i013p02165

Jørgensen, T. S., Friis-Christensen, E., & Wilhjelm, J. (1972). Interplanetary magnetic-field direction and high-latitude ionospheric currents. *Journal of Geophysical Research*, *77*(10), 1976–1977. doi: https://doi.org/10.1029/JA077i010p01976

Khan, H., & Cowley, S. (1999). Observations of the response time of high-latitude ionospheric convection to variations in the interplanetary magnetic field using EISCAT and IMP-8 data. *Annales Geophysicae*, *17*(10), 1306–1335. doi: https://doi.org/10.1007/s00585-999-1306-8

King, J., & Papitashvili, N. (2005). Solar wind spatial scales in and comparisons of hourly Wind and ACE plasma and magnetic field data. *Journal of Geophysical Research: Space Physics*, *110*(A2). doi: https://doi.org/10.1029/2004JA010649

Lockwood, M., & McWilliams, K. A. (2021). On optimum solar wind–magnetosphere coupling functions for transpolar voltage and planetary geomagnetic activity. *Journal of Geophysical Research: Space Physics*, e2021JA029946. doi: https://doi.org/10.1029/2021JA029946

Mansurov, S. (1969). New evidence of a relationship between magnetic fields in space and on earth. *Geomag. Aeron.*, *9*, 622–623.

Milan, S., Baddeley, L., Lester, M., & Sato, N. (2001). A seasonal variation in the convection response to IMF orientation. *Geophysical Research Letters*, *28*(3), 471–474. doi: https://doi.org/10.1029/2000GL012245

Milan, S., Carter, J., Korth, H., & Anderson, B. (2015). Principal component analysis of Birkeland currents determined by the Active Magnetosphere and Planetary Electrodynamics Response Experiment. *Journal of Geophysical Research: Space Physics*, *120*(12), 10–415. doi: https://doi.org/10.1002/2015JA021680

Milan, S., Carter, J., Sangha, H., Laundal, K., Østgaard, N., Tenfjord, P., ... others (2018). Timescales of dayside and nightside field-aligned current response to changes in solar wind-magnetosphere coupling. *Journal of Geophysical Research: Space Physics*, *123*(9), 7307–7319. doi: https://doi.org/10.1029/2018JA025645

Milan, S., Clausen, L., Coxon, J., Carter, J., Walach, M.-T., Laundal, K., ... others (2017). Overview of solar wind–magnetosphere–ionosphere–atmosphere coupling and the generation of magnetospheric currents. *Space Science Reviews*, *206*(1-4), 547–573. doi: https://doi.org/10.1007/s11214-017-0333-0

Milan, S., Gosling, J., & Hubert, B. (2012). Relationship between interplanetary parameters and the magnetopause reconnection rate quantified from observations of the expanding polar cap. *Journal of Geophysical Research: Space Physics*, *117*(A3).

Newell, P., Sotirelis, T., Liou, K., Meng, C.-I., & Rich, F. (2007). A nearly universal solar wind-magnetosphere coupling function inferred from 10 magnetospheric state variables. *Journal of Geophysical Research: Space Physics*, *112*(A1).

Svalgaard, L. (1973). Polar cap magnetic variations and their relationship with the interplanetary magnetic sector structure. *Journal of Geophysical Research*, *78*(13), 2064–2078. doi: https://doi.org/10.1029/JA078i013p02064

Waters, C., Anderson, B., Green, D., Korth, H., Barnes, R., & Vanhamäki, H. (2020). Science data products for AMPERE. In *Ionospheric Multi-Spacecraft Analysis Tools* (pp. 141–165). Springer, Cham. doi: https://doi.org/10.1007/978-3-030-26732-2_7

Waters, C., Anderson, B., & Liou, K. (2001). Estimation of global field aligned currents using the Iridium® system magnetometer data. *Geophysical Research Letters*, *28*(11), 2165–2168. doi: https://doi.org/10.1029/2000GL012725